Bioactive Materials 12 (2022) 120–132

Contents lists available at ScienceDirect

Bioactive Materials

journal homepage: www.keaipublishing.com/en/journals/bioactive-materials

3D-printed bioactive ceramic scaffolds with biomimetic micro/nano-HAp surfaces mediated cell fate and promoted bone augmentation of the bone–implant interface *in vivo*

Xiao Liu [a,b,c,1], Yali Miao [b,d,e,1], Haifeng Liang [f], Jingjing Diao [a,b,g], Lijing Hao [a,b,c,d,e], Zhifeng Shi [a,b,g], Naru Zhao [a,b,c,d,e,**], Yingjun Wang [a,b,c,d,e,h,*]

[a] National Engineering Research Center for Tissue Restoration and Reconstruction, Guangzhou, China
[b] School of Materials Science and Engineering, South China University of Technology, Guangzhou, 510641, China
[c] Guangdong Province Key Laboratory of Biomedical Engineering, South China University of Technology, Guangzhou, 510006, China
[d] Key Laboratory of Biomedical Materials and Engineering of the Ministry of Education, South China University of Technology, Guangzhou, 510006, PR China
[e] Innovation Center for Tissue Restoration and Reconstruction, South China University of Technology, Guangzhou, 510006, PR China
[f] Department of Orthopedics, Zhujiang Hospital, Southern Medical University, No. 253 Industrial Avenue, Haizhu, Guangzhou, 510280, People's Republic of China
[g] Medical Devices Research & Testing Center of SCUT, Guangzhou, 510006, PR China
[h] Bioland Laboratory (Guangzhou Regenerative Medicine and Health Guangdong Laboratory), 510005 Guangzhou, China

ARTICLE INFO

Keywords:
3D printed porous scaffold
Bioactive ceramics
HAp surface layer
Cell fate mediation
Bone augmentation

ABSTRACT

Calcium phosphate bio-ceramics are osteo-conductive, but it remains a challenge to promote the induction of bone augmentation and capillary formation. The surface micro/nano-topography of materials can be recognized by cells and then the cell fate are mediated. Traditional regulation methods of carving surface structures on bio-ceramics employ mineral reagents and organic additives, which might introduce impurity phases and affect the biological results. In a previous study, a facile and novel method was utilized with ultrapure water as the unique reagent for hydrothermal treatment, and a uniform hydroxyapatite (HAp) surface layer was constructed on composite ceramics (β-TCP/$CaSiO_3$) *in situ*. Further combined with 3D printing technology, biomimetic hierarchical structure scaffolds were fabricated with interconnected porous composite ceramic scaffolds as the architecture and micro/nano-rod hybrid HAp as the surface layer. The obtained HAp surface layer favoured cell adhesion, alleviated the cytotoxicity of precursor scaffolds, and upregulated the cellular differentiation of mBMSCs and gene expression of HUVECs *in vitro*. *In vivo* studies showed that capillary formation, bone augmentation and new bone matrix formation were upregulated after the HAp surface layer was obtained, and the results confirmed that the fabricated biomimetic hierarchical structure scaffold could be an effective candidate for bone regeneration.

1. Introduction

Biomaterials have great expectations in guiding cell fate and regulating the commitment of cell lineages [1]. Current biomaterials for bone regeneration can be endowed with osteo-conductivity, but it is still a challenge to promote the induction of bone augmentation and capillary formation and even achieve osteo-inductivity. The surface micro/nano-topography of these materials can be translated as biological cues by cells, mediating the epigenetic states of cells [2,3]. It has been suggested that cellular adhesion, cytoskeleton, self-renewal and focal adhesion kinase are regulated by surface micro/nano-topography [4,5], which are related to the activation of certain signalling pathways, such as Wnt [6], ERK 1/2 [7] and p38 MAPK [8]. However, many studies have been based on bioinert materials as model materials, such as metallic arrays [9] and organic patterns [10,11], since it is still a challenge to carve the micro/nano-structure on

Peer review under responsibility of KeAi Communications Co., Ltd.
* Corresponding author. National Engineering Research Center for Tissue Restoration and Reconstruction, Guangzhou, China.
** Corresponding author. School of Materials Science and Engineering, South China University of Technology, Guangzhou, 510641, China.;
E-mail addresses: nrzhao@scut.edu.cn (N. Zhao), imwangyj@163.com (Y. Wang).
[1] The author contributed equally to the work.

https://doi.org/10.1016/j.bioactmat.2021.10.016
Received 12 August 2021; Received in revised form 30 September 2021; Accepted 14 October 2021
Available online 22 October 2021

the surface of brittle and unmanageable bio-ceramics [12]. Although these studies might have uncovered how the metallic and organic surface texture of the materials could be translated as biological cues and mediate cell fate, the results did not elucidate the effects between inorganic surface structure and cellular behaviours. Furthermore, bio-ceramics are potential candidates for bone regeneration due to their adaptable mechanical properties, biocompatibility, bioactivity and osteo-conductivity [13], and it is meaningful to investigate the biological effects of micro/nano-coatings on bioactive ceramic surfaces.

To carve micro/nano-structures on bio-ceramics, common methods involve organic additives [1,14,15] and mineralization reagents [16,17]. However, the obtained crystals might contain impure phases, and additives might interfere with the biological results. In a previous study, when β-tricalcium phosphate (β-TCP) was soaked in simulated body fluid, the obtained surface crystal phase was Mg-whitlockite (WH, $Ca_{18}Mg_2(HPO_4)_2(PO_4)_{12}$) [18] instead of hydroxyapatite (HAp), whose components are similar to the inorganic components of natural bone; HAp is a stable phase of CaP ceramics and has been widely utilized as a coating to improve the osseointegration of substrates [19]. However, traditional processes employ mineral solutions, which results in additional influencing factors. Hence, a facile hydrothermal reaction system without organic additives and mineralization reagents was utilized in previous work [20]. β-TCP is a biodegradable ceramic that can provide a surface with a low interfacial energy with apatite [21], and $CaSiO_3$ can provide active sites for heterogeneous nucleation and is inclined to form HAp [22,23]. Hence, a micro/nano-HAp surface layer was constructed *in situ* on a β-TCP/$CaSiO_3$ bio-ceramic tablet after hydrothermal treatment in ultrapure water. Osteogenesis emerges in porous materials [24], and interconnected porosity is necessary for a material to be osteo-inductive by providing space for cell migration and tissue ingrowth [13]. Hence, 3D scaffolds were used as the pre-treated original substrate. Moreover, the 3D printing technique, with the characteristics of high precision and accuracy, has been utilized to fabricate porous bio-ceramic scaffolds that might be candidates for bone regeneration [25]. These 3D printing techniques play an important role in personalized bone regeneration as well as precision medicine [26]. From this perspective, 3D-printed scaffolds were utilized to construct the architecture of the substrate. In addition, in this study, a 3D bioplotter was utilized in this article since, compared to another 3D printing technique, this system possesses the advantage of fabricating 3D scaffolds with a high solid content; the size [27], synthetic process and component proportion of β-TCP/$CaSiO_3$ were based on our previous work [28]. 3D scaffolds (β-TCP/$CaSiO_3$) with interconnected pores were fabricated via an extrusion moulding 3D Bioplotter™ system (Regenovo, China). The natural bone surface was long axis growth micro/nano-HAp crystals with poor crystallization [29]; Hence, the surface was modified to long axis growth micro/nano-rod HAp crystals with poor crystallization (compared to sintered crystals). By means of 3D printing technology and hydrothermal mineralization, the macro-architecture and micro/nano-surface structure of scaffolds were constructed, and the fabricated biomimetic hierarchical structure scaffolds exhibited a micro/nano-HAp surface layer and interconnected porous architecture.

Since angiogenesis and osteogenesis have been proven to be coupled [30], it has been indispensable to investigate the effects of biomaterials on these two processes. Some studies focused on the angiogenesis differentiation of adipose [6,31] or bone marrow-derived mesenchymal stem cells (MSCs) [1,8,32,33], but whether the materials can regulate the cellular behaviours of endothelial cells remains to be elucidated. In addition, some studies reported that cell recruitment and paracrine between MSCs and pericytes were the key to osteogenesis [34]; these results might suggest that angiogenesis was the result of the effects between materials and endothelial cells rather than direct angiogenesis differentiation of MSCs. Hence, human umbilical vein endothelial cells (HUVECs) and mouse bone mesenchymal stem cells (mBMSCs) were utilized to investigate the effects of the micro/nano-HAp surface layer on angiogenesis and osteogenic differentiation *in vitro*. Furthermore, calcium phosphate (CaP)-based bio-ceramics have been proven to be osteo-conductive [13] and have shown the capacity to regenerate bone tissue in bone defect environments. Nevertheless, it was intriguing and meaningful to promote the bone augmentation ability, namely, to form new bone out of cortical bone without any bone defect [35]. A bone augmentation process is necessary for bone regeneration, especially for alveolar bone, but without adding any biomolecules or establishing blood express way [36,37], it remains a challenge to achieve bone augmentation with bio-ceramics. Therefore, the capacity for bone augmentation was measured via ectopic implantation without any bone defect. Therefore, in this study, *in vivo* studies were performed in Sprague–Dawley (SD) rat subcutaneous implants in the backs and skull near the calvaria. The brief illustration of the study was shown in Scheme 1.

2. Materials and methods

2.1. Fabrication of biomimetic hierarchical structure scaffolds

The synthesis of the particles [20] and the fabrication of the scaffolds [28] were based on previous studies. The process in brief was as follows:

β-TCP synthesis. The ratio of calcium (Ca) to phosphate (P) was 3/2. The initial concentrations of Ca-nitrate and $(NH_4)_2HPO_4$ were 0.45 M and 0.5 M, respectively. Polyethylene glycol (PEG, MW 6000) was utilized as a dispersant and added to Ca-nitrate solution. Ammonium hydroxide solution was used to modulate the pH of the solution. The pH was regulated to approximately 6.8, and the particles were lyophilized and heat-treated at 850°C for 3 h.

HAp synthesis. The processes were similar to those of β-TCP synthesis. Briefly, the ratio of Ca to P was 5/3, and the pH of the reaction system was modulated between 9.6 and 10.0 with ammonium hydroxide. The particles were lyophilized and heat-treated at 850°C for 3 h.

$CaSiO_3$ synthesis. The ratio of Ca to silica (Si) was 1/1; 0.5 M Ca-nitrate and 0.5 M sodium *meta*-silicate were mixed with 0.0025 M PEG, which served as a dispersant. Calcination was performed at 1100°C for 3 h.

Scaffold fabrication. 3D printing technology (3D-Bioplotter TM system, Regenovo, Hangzhou) was used. The slurry for printing was prepared by mixing the inorganic powders into a mixture of distilled water and glycerol; then, ammonium polyacrylate was added as a dispersant. A QM-BP planetary ball mill (Nanjing Nanda Instrument Plant, China) was used to mix the slurry. Hydroxypropylmethyl cellulose was used to improve the viscosity, octanol was added to eliminate foaming of the slurry, and the architecture of the scaffolds was designed via the 3D CAD software SolidWorks. The slurry for 3D printing was extruded with a pressure of 3–4 bar at a speed of 4–6 mm s^{-1}, and the tapered tip for printing (Nordson EFD, USA) was 250 μm. Before thermal treatment, the 3D-printed scaffolds were dried at room temperature for 2 d. The dried scaffolds were then calcined at 1100°C for 3 h. Interconnected porous 3D scaffolds with a diameter of 10 mm and height of 2.5 mm were fabricated as pre-treated original scaffolds (designated Os) [28]. The composition of the scaffolds was β-TCP with 15 wt% $CaSiO_3$. Micro/nano-HAp surface layers were obtained on 3D scaffolds after hydrothermal treatment of the pre-treated original scaffolds at 120°C for 24 h and were designated NMs based on a previous study [20]. In this article, the aqueous solution was ultrapure water, with a pH value of 4, and orthophosphoric acid was utilized as the pH adjustment reagent. The HAp scaffolds and β-TCP scaffolds were set as the control groups and designated Hs and Ts, respectively.

2.2. Material characterization

Surface crystal phase characterization: For X-ray diffraction (XRD), X-ray scanning was performed from 5 to 80°, the scanning step length and rate were 0.02° and 1°/min, respectively. Material morphology was observed by field emission scanning electron microscopy (SEM, MERLIN, ZEISS). Before observation, sputtering platinum treatment was

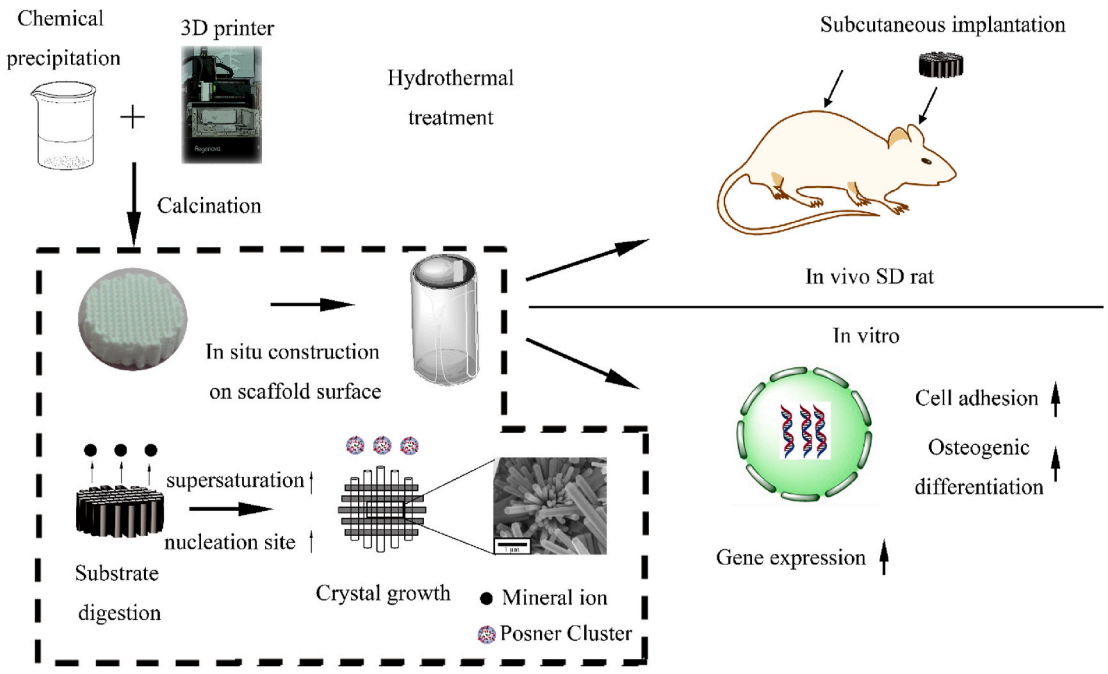

Scheme 1. Brief illustration of the study.

performed on the surface of the samples. The micro-structure of the surface crystal was measured via transmission electron microscopy (TEM), and the specific surface area was measured by Brunauer–Emmett–Teller (BET) adsorption/desorption isotherm determination.

2.3. Cell culture and seeding

Primary mouse bone mesenchymal stem cells (mBMSCs) were purchased from ATCC, while human umbilical vein endothelial cells (HUVECs) were purchased from ScienCell. The cells used in the cell experiment were mBMSCs at passages 3–6 and HUVECs at passages 3–4. The culture medium for mBMSCs was Dulbecco's minimal Eagle medium (DMEM) high-glucose medium containing 1% double antibody (penicillin-streptomycin) and 10% foetal bovine serum (FBS). HUVECs were cultured in endothelial cell medium (ECM) with 1% endothelial cell growth supplement (ECGS), 1% double antibody (penicillin-streptomycin) and 5% FBS. The cells were digested and isolated by 0.25% ethylenediaminetetraacetic acid (EDTA)-trypsin. Before seeding, materials were sterilized in an autoclave (121°C, 30 min) and soaked in phosphate buffer overnight. When seeding, a high concentration cell suspension was added onto the surface of scaffolds. The cells were distributed over the whole surface. Then, culture medium was added after cells adhered preliminarily (approximately 1 h). In addition, the medium for osteogenic differentiation included osteogenesis-inducing reagents mixed with 100 nM dexamethasone, 10 mM β-glycerophosphate and 50 mM ascorbic acid.

2.4. Cell proliferation

The scaffolds for cell culture were 3D, and it was difficult to calculate the area. Therefore, the units of cell culture were the cell number per scaffold. Cell Counting Kit 8 (CCK-8) was utilized to detect cell proliferation after the cells (5×10^4 per scaffold) were seeded onto the surface of scaffolds for 1 d, 3 d and 5 d. Before testing, the medium was removed and rinsed with phosphate buffer 3 times. A total of 330 mL of CCK-8 working solution (the ratio of CCK-8 stock solution to medium was 1:10) was added to each sample. After being placed in an incubator for 1 h, 100 mL of supernatant was transferred to a 96-well plate and measured in a microplate reader (wavelength 450 nm).

2.5. Cellular differentiation of mBMSCs and gene expression of HUVECs

mBMSCs (3×10^5 per scaffold) were cultured in DMEM for 2 d and then cultured in the presence of osteogenesis-inducing reagents. Before RNA extraction, the medium was removed and rinsed 3 times in phosphate-buffered saline (PBS). TRIZOL was utilized to induce cell lysis. Chloroform and isopropanol were used to collect RNA. The collected RNA was normalized via a spectrophotometer. Reverse transcription primer sequences for RT-PCR and the test system were established according to a previous study [20]. The results of gene expression were estimated by $2^{-\Delta\Delta Ct}$. For HUVECs, cells were cultured in ECM for 7 d since the cell viability was decreased after 7 passages. The PCR processes were the same as those for mBMSCs. The primer sequences are listed in Tables 1 and 2. GAPDH was used as a housekeeping gene.

2.6. Cellular adhesion

Cellular adhesion on the surface was observed via SEM, and quantitative characterization was measured by detecting the expression of integrin subunits α_2, α_5, α_v and β_1. After mBMSCs (3×10^5 per scaffold) were seeded on the surface for 12 h, the expression of integrin subunits was tested. The process of RNA extraction was the same as that described above, and the primer sequences are shown in Table 3.

Table 1
Primer sequences for RT-PCR mBMSCs.

Gene	Direction	Sequence (5′-3′)
GAPDH	Forward	TGTGTCCGTCGTGGATCTGA
	Reverse	TTGCTGTTGAAGTCGCAGGAG
OPN	Forward	TGCAAACACCGTTGTAACCAAAAGC
	Reverse	TGCAGTGGCCGTTTGCATTTCT
OCN	Forward	AGCAGCTTGGCCCAGACCTA
	Reverse	TAGCGCCGGAGTCTGTTCACTAC
OSX	Forward	CGTCCTCTCTGCTTGAGGAA
	Reverse	CTTGAGAAGGGAGCTGGGTA
Col-I	Forward	ATGCCGCGACCTCAAGATG
	Reverse	TGAGGCACAGACGGCTGAGTA

Table 2
Primer sequences for RT-PCR HUVECs.

Gene	Direction	Sequence (5′-3′)
GAPDH	Forward	GCACCGTCAAGGCTGAGAACA
	Reverse	TGGTGAAGACGCCAGTGGA
CD31	Forward	CCGCATATCCAAGGTCAGCA
	Reverse	CACCTTGGTCCAGATGTGTGAA
KDR	Forward	AGCCAGCTCTGGATTTGTGGA
	Reverse	CATGCCCTTAGCCACTTGGAA
TGF-β	Forward	TCCTGGCGATACCTCAGCAA
	Reverse	GCTAAGGCGAAAGCCCTCAA
VEGF	Forward	CATCCAATCGAGACCCTGGTG
	Reverse	TTGGTGAGGTTTGATCCGCATA

Table 3
Primer sequences for integrin subunit RT-PCR.

Gene	Direction	Sequence (5′-3′)
GAPDH	Forward	TGTGTCCGTCGTGGATCTGA
	Reverse	TTGCTGTTGAAGTCGCAGGAG
α_2	Forward	TGCCTACTTGTGTGGCGTGAA
	Reverse	TCACCCGAGTGGTAGTCACAATG
α_5	Forward	TGAACTGCACGGCAGATACAGAG
	Reverse	ATCCCGCTTGGTGATGAGATG
α_v	Forward	TGCAGTGGTTCGGAGCAACCCTA
	Reverse	TTTTCTGTGCGCCAGCTATAC
β_1	Forward	ATCATGCAGGTTGCGGTTTG
	Reverse	GGTGACATTGTCCATCATTGGGTA

2.7. Immunofluorescent staining

Osteocalcin (OCN) secretion in mBMSCs and platelet-endothelial cell adhesion molecule (CD31) in HUVECs were characterized via immunofluorescent staining with a cell density of 3×10^5 per scaffold. After rinsing with phosphate buffer 3 times, the samples were fixed in paraformaldehyde solution for 30–60 min. Next, 1 mL of 0.1% Triton X-100 and 3% bovine serum albumin (BSA) solution were added to the samples for 15–20 min and 60 min, respectively, to change the cell permeability and seal the cytomembrane. OCN antibody incubation was used to stain the OCN secretion of mBMSCs, and CD31 antibody incubation was used to stain CD31 in HUVECs. F-actin and 4′,6-diamidino-2-phenylindole (DAPI) were utilized to stain the cytoskeleton and nucleus, respectively. The samples were observed via laser scanning confocal microscopy.

2.8. In vivo surgery and evaluation

All protocols, surgery processes, aseptic operation and postoperative antibiotics were approved by the Ethics Committee of Southern Medical University. The extramembranous osteogenesis was placing the scaffolds into subcutaneous site on the skull [38] of SD rats. The implanted scaffolds with 10 mm diameter and 2.5 mm height were used. The scaffolds were placed on the periosteum gently. The specimens were retrieved after implanting for 4 and 8 weeks. A total of 24 male SD rats with weight range from 180 to 200 g were anesthetized with 4% chloral hydrate whose dose was 1 mL/100 g.

As for the ectopic subcutaneous implantation of SD rats were to value the angiogenesis of the scaffolds in the environment without stem cells. The scaffolds were implanted into the back of the rats. The process was similar with that of extramembranous osteogenesis experiments on the skull.

Before measuring, 4% paraformaldehyde solution was used to fix the harvested specimens. The decalcified process was resort to neutral 10% ethylene diamine tetraacetic acid (EDTA). The results were evaluated via histologic section: hematoxylin-eosin staining, Masson staining and immunohistochemical staining of Platelet endothelial cell adhesion molecule (CD31) and osteocalcin (OCN). Micro-CT was also utilized to observe the bone formation.

2.9. Statistical analysis method

Data were shown as the mean values ± standard deviation. Single analysis of variance at $p < 0.05$ was used to indicate statistical significance. The label * was used to indicate statistical significance. Special note: the # represents the significant differences compared to control groups.

3. Results

3.1. Surface morphology of 3D scaffolds

Through the 3D-bioplotting technology, the fabricated scaffolds were endowed with interconnected pores. The diameter of extruded bioceramic fibres was approximately 250 μm, and the pore size was approximately 250 μm. After hydrothermal treatment for 24 h, micro/nano-rod and rod-cluster crystals were formed *in situ* at the surface of the precursor scaffold (Fig. 1A and B). The surface crystal was hexagonal, and the size of the constructed crystals was uniform.

The obtained rod-cluster micro/nano-crystals on the surface were peeled and observed via TEM (Fig. 1C). Crystals were observed on carbon film. The lattice of the selected area electron diffraction pattern indicated that the crystal was a single crystal. In addition, the surface diffraction fringe was obvious, and some nanoscale “pellets” could be seen on the surface of nanorods by high-resolution TEM (HR-TEM). The “pellets” indicated that the crystal growth process might involve building unit accumulation on the crystals rather than a direct phase transition to HAp.

The 3D scaffolds with a micro/nano-crystal surface layer were endowed with a higher specific surface area than that of the pre-treated original scaffolds. The adsorption isotherm was type II, and the hysteresis loop was type H3, which was attributed to the irregular pore structure. The surface pore area (Fig. 1D inset) shows that the amounts of meso-pores (2-50 nm) and macro-pores (greater than 50 nm) on NMs increased.

3.2. Surface phase and element composition

The XRD diffraction pattern of Os matched the standard JCPDS code of whitlockite, and the most intense diffraction peak of $CaSiO_3$ at 30.06° corresponding to the crystal plane (302) was not obvious due to the low content. According to XRD (Fig. 2A), the crystal phase of the hydrothermally treated surface was HAp. The peaks at 25.90°, 31.80°, 32.18°, 33.00° and 34.09° corresponded to the HAp crystal planes (002), (121), (112), (300) and (202), respectively, and the code of standard JCPDS is shown in the inset. From energy dispersive X-ray spectroscopy (EDS) measurements, elemental analysis confirmed that the composition of the surface crystal was pure HAp. The elements were uniformly distributed on the surface, and the ratio of Ca and P was approximately 1.60.

3.3. The cellular adhesion

Integrin is composed of coupled subunits, and the target genes in this study were α_2, α_5, α_v and β_1 as shown in Fig. 3. The expression of these genes could reflect cellular adhesion on the scaffolds. Compared to Os, NMs upregulated the expression of subunits α_2, α_5, and α_v. In addition, the gene expression of α_2 and α_5 was more upregulated with NMs than with Hs, but no significant difference emerged in the expression of β_1 among the Hs, Os and NMs groups. The results indicated that cellular adhesion was upregulated in NMs.

3.4. Cell proliferation

mBMSCs proliferation was measured via CCK-8 and the results were shown in ESI Fig. 3. The β-TCP scaffolds (designated as Ts) were used as positive control groups. When cultured for 1 d, no significant differences

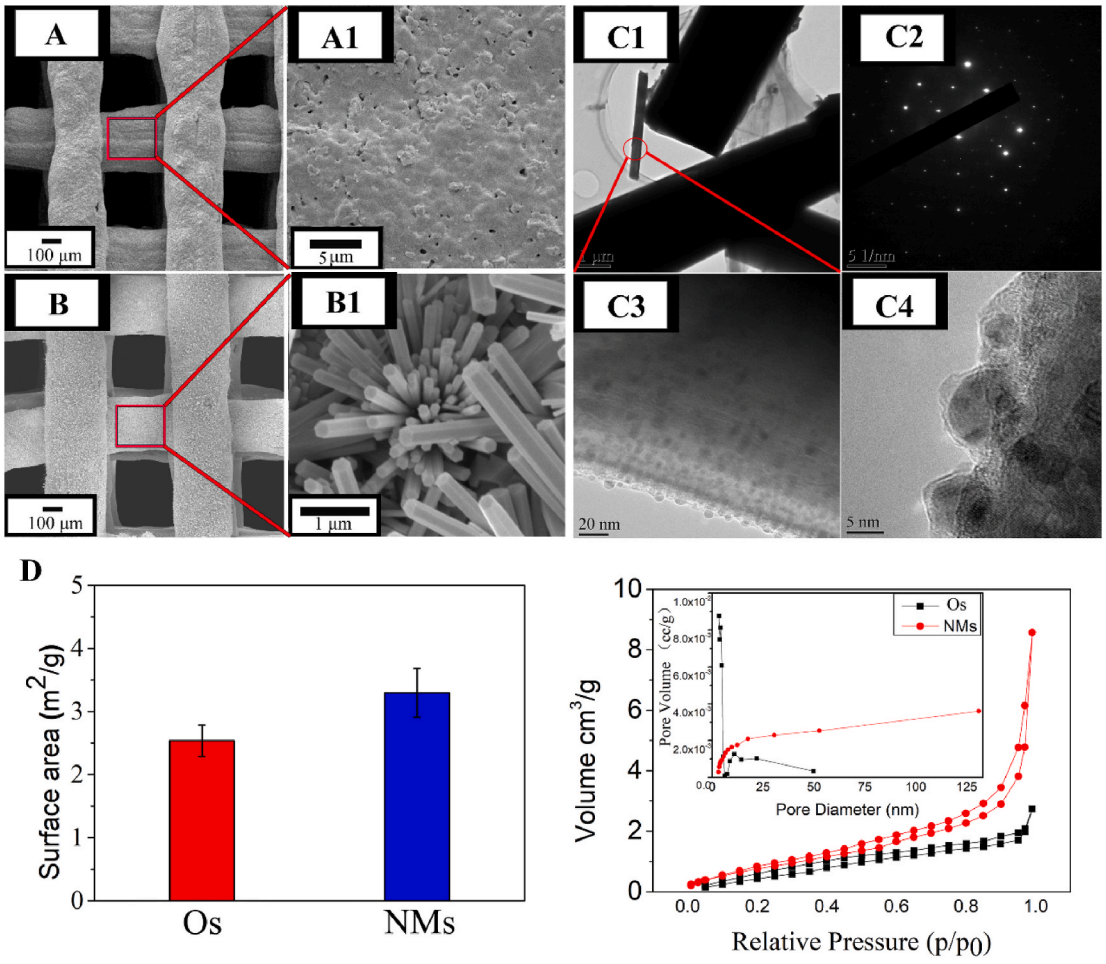

Fig. 1. (A) and (A1) show the pre-treated original scaffolds (Os). (B) and (B1) show the surface micro/nano-structure of 3D scaffolds (NMs) via hydrothermal treatment in ultrapure water for 24 h at 120°C. TEM of the obtained micro/nano-hydroxyapatite crystals. The obtained crystals were peeled from the surface. (C1) TEM image on carbon film. (C2) Selected area electron diffraction (SAED). (C3) High-resolution transmission electron microscopy (HR-TEM). (C4) HR-TEM image of the margin. BET measurements of the surface. (D) Specific surface area of Os and NMs and the associated nitrogen adsorption–desorption isotherms. The inset picture shows the micro-pore volume distribution.

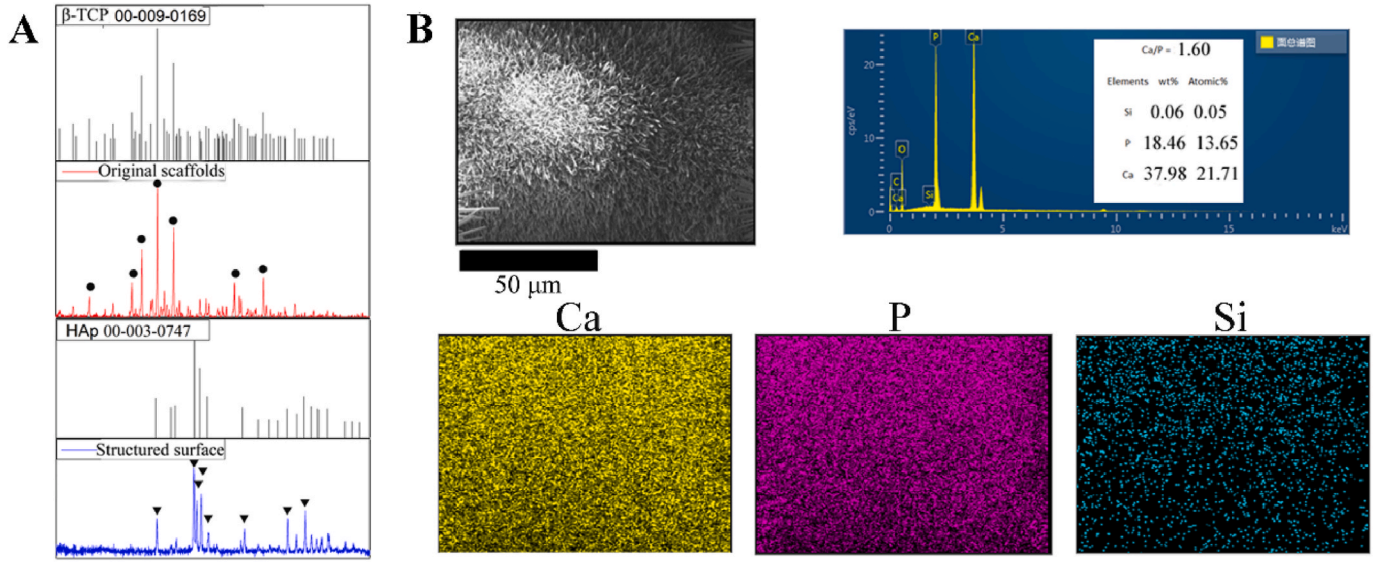

Fig. 2. (A) XRD measurement on the surface of Os and NMs. The code of standard JCPDS is shown in the inset; circles represent the peak of β-TCP, while triangles correspond to HAp. (B) EDS mapping of the surface elements. The listed elements are calcium, phosphorus and silicon, with Ca/P = 1.60.

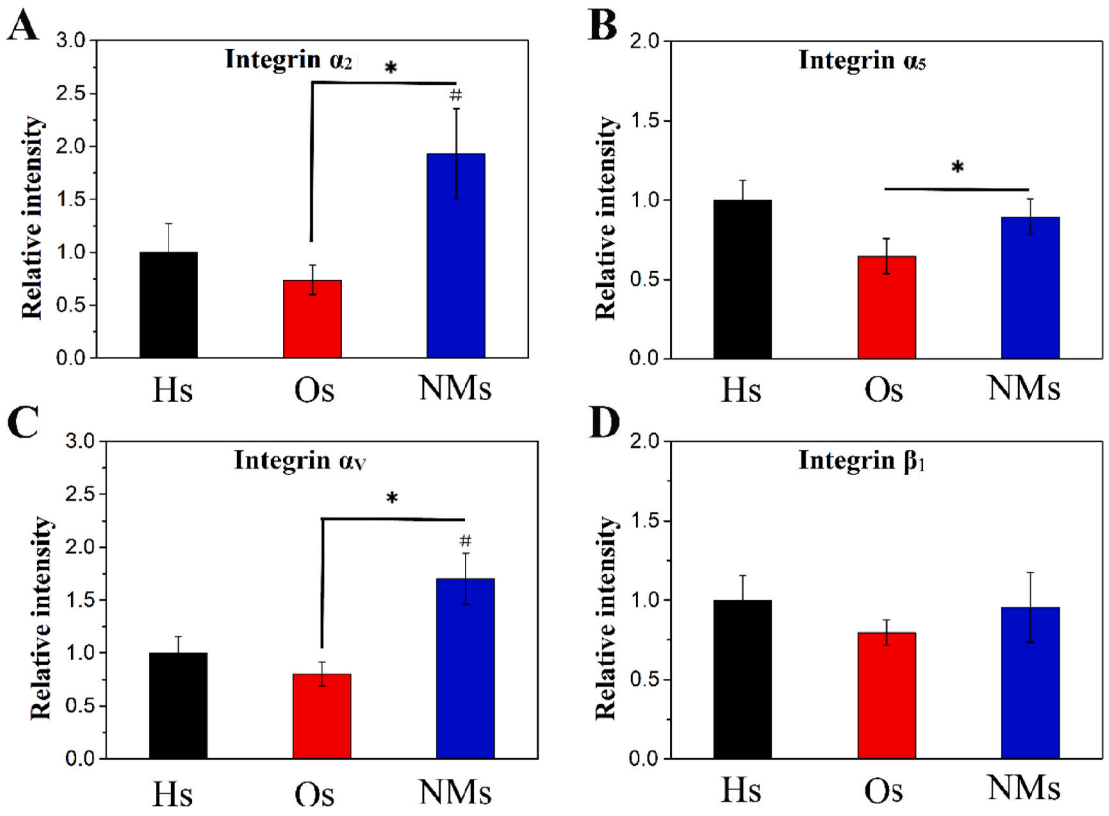

Fig. 3. Gene expression of integrins after culturing mBMSCs in DMEM for 12 h. The measured subunits are (A) α_2, (B) α_5, (C) α_v and (D) β_1.

were observed. The cell proliferation of NMs was slightly upregulated when cultured for 3 d. However, no significant differences in cell proliferation were noted between the groups, even after culturing for 7 d. The effects on mBMSCs proliferation were similar among Hs, Ts, Os and NMs. Regarding HUVECs, no significant difference emerged among Hs, Ts and NMs, while Os slightly inhibited HUVECs proliferation when cultured for 3 d and 5 d.

3.5. Osteogenic differentiation

From the RT-PCR results in Fig. 4, the gene expression of OSX in NMs was higher than that in Ts and Os but showed no significant differences compared to the control group (Hs) after culturing for 7 d. When cultured for 14 d, OSX gene expression was not significantly different between the Ts, Os and NMs groups but showed significantly higher upregulation than that in the Hs group. Col-I gene expression in the NMs group was significantly lower than that in the Os groups when cultured for 7 d. With the culture time prolonged to 14 d, Col-I gene expression in the NMs group was more upregulated than that in the other groups. The gene expression of OCN shared a similar tendency with Col-I gene expression. Regarding OPN gene expression, no significant differences were observed at the initial stage. After culturing for 14 d, the gene expression of OPN in the NMs group was higher than that in the other groups. The results indicated that the analysed osteogenic genes were

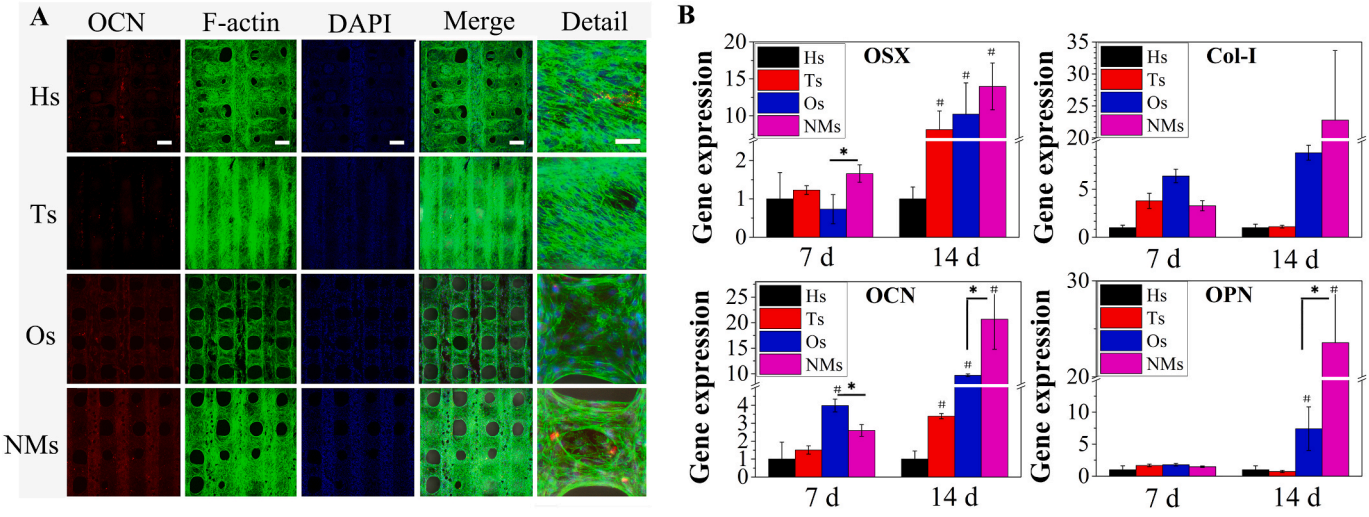

Fig. 4. (A) Immunofluorescence of osteocalcin on scaffolds, DMEM culture for 2 d and osteogenic medium culture for 12 d. Scale bar 200 μm. Detail with 50 μm as the scale bar. (B) mBMSCs osteogenic differentiation on the scaffolds. The targeted gene markers were OSX, Col-I, OCN and OPN.

upregulated in NMs, and the upregulation effects were more obvious as the culture time was prolonged to 14 d. The protein secretion was a supplement to transcriptional level measurement. Immunofluorescence was used to measure secretion of the analysed proteins, and F-actin and DAPI staining were also utilized. After culturing for 14 d (Fig. 4A), mBMSCs were distributed over the whole surface of the scaffolds in the Hs, Ts, Os and NMs groups since bioactive inorganic materials favour the adhesion and proliferation of stem cells. In addition, mBMSCs tended to reside on the upper surface in Hs and Ts but tended to wrap the surface fibre in Os and NMs. For OCN immunofluorescence, few dots emerged in the Ts and Os groups, but considerable fluorescence was observed in the Hs and NMs groups.

As for the effects on the gene expression of angiogenic marker in HUVECs, the target genes were CD31, KDR, TGF-β and VEGF as shown in Fig. 5. The gene expression of VEGF and its receptor KDR were more up-regulation in NMs than that of Hs, Ts and Os. Besides, except no significant differences in the expression of TGF-β, the gene expression of CD31 were up-regulated in NMs than that of other groups. Furthermore, no significant trend emerged among Hs, Ts and Os which indicated the ion release might show negligible effects on the HUVECs gene expression. The results might be attributed to the obtained micro/nano HAp surface layer which could form a suitable niche for HUVECs.

Regarding immunofluorescence analysis, the targeted protein for HUVECs was CD31, combined with DAPI and F-actin staining (Fig. 5A). The cells on Hs, Ts and NMs were observed to wrap the fibre, while there were fewer cells on Os than in the other groups. For CD31 immunofluorescence, fluorescence appeared in the Hs, Ts, Os and NMs groups, but the fluorescence observed on NMs was more considerable, and cells accumulated on the surface in the NMs group. In addition, the immunofluorescence results confirmed that although mBMSCs proliferation was not significantly different among the groups, a decrease in the number of HUVECs was observed in Os.

3.6. *In vivo extramembranous ectopic implantation*

From micro-CT observation (ESI Fig. 2), the scaffolds in NMs bonded to bone, and the osseointegration was observed from histological sections; however, no similar phenomena was observed in the other groups.

From H&E staining (Fig. 6A), fibrous tissue with obvious erythrocytes was distributed on Hs after implanting for 4 weeks. With the implantation time prolonged to 8 weeks, no new bone matrix formed, but some capillary structure emerged. The Ts and Os groups exhibited the same tendency. After implanting for 4 and 8 weeks, no new bone matrix emerged in the Ts and Os groups. For the NMs scaffolds, a tight bond was formed at the bone–implant interface after implanting for 4 weeks, with a bone-like matrix appearing at the radial edge of the scaffolds. After implanting for 8 weeks, the surface of the scaffold was embedded with new bone matrix, which indicated that bone augmentation was promoted. In addition to bone augmentation at the bone–implant interface, new bone matrix was found at the inner pores of NMs.

According to Masson staining (Fig. 6B), no collagen fibres were found on the surface of the Hs group after 4-week implantation, and a small amount of collagen fibres was found after 8-week implantation, with partial capillary structure. In the Ts group, there was some collagen fibres after implanting for 4 weeks, while after implanting for 8 weeks, the amount of collagen fibres increased, and some capillary structure also appeared. In the Os group, the considerable collagen fibres and capillary structures emerged till implanting for 8 weeks. Although the amount of collagen increased with the implantation time from 4 to 8 weeks in the Hs, Ts and Os groups, no new bone matrix appeared. In the NMs group, collagen fibres were secreted significantly on the surface of periosteum after implantation for 4 weeks, and the matrix at the radial edge of the scaffold contained considerable collagen. After implantation for 8 weeks, more collagen fibres were secreted, which might suggest maturation of the new bone matrix.

Immunostaining of OCN in Fig. 7 showed that no OCN was secreted on the surface of scaffolds in the Hs group after 4 weeks of implantation, and there was a small amount of OCN after 8 weeks of implantation. In the Ts group, a slight amount of OCN was noted after implanting for 4 weeks, but the OCN secretion increased after implanting for 8 weeks. In the Os group, the positive area was higher than that in the Hs and Ts groups, and the secretion was close to that in the NMs group. However, the average optical (AO) values were inferior to those of NMs. In the NMs group, OCN was secreted significantly after 8 weeks of implantation. Moreover, the positive area and AO value were relatively higher than that of other scaffolds.

3.7. *In vivo ectopic subcutaneous implantation*

In vivo ectopic subcutaneous implantation was performed at the back of SD rats. After implanting the scaffolds for 4 weeks, considerable capillaries could be found in NMs, as shown in Fig. 8A, and flat haemocytes were distributed in the capillaries. Few capillaries were observed in the Hs, Ts and Os groups. The results of ectopic subcutaneous implantation in the backs of SD rats corresponded to those of the effects on endothelial cells. Furthermore, the capillaries regressed after

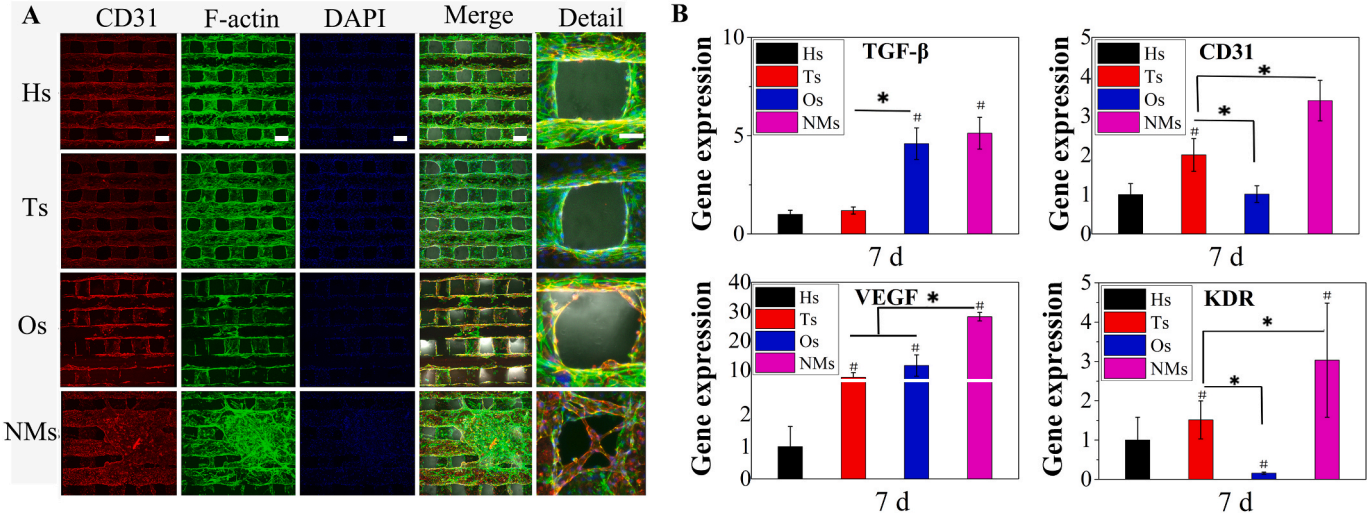

Fig. 5. (A) Immunofluorescence of CD31 on scaffolds and HUVECs cultured for 7 d in ECM. Scale bar 200 μm. Detail with 50 μm as the scale bar. (B) Gene expression of angiogenesis markers in HUVECs cultured on scaffolds for 7 d. Targeted gene markers were CD31, KDR, TGF-β and VEGF.

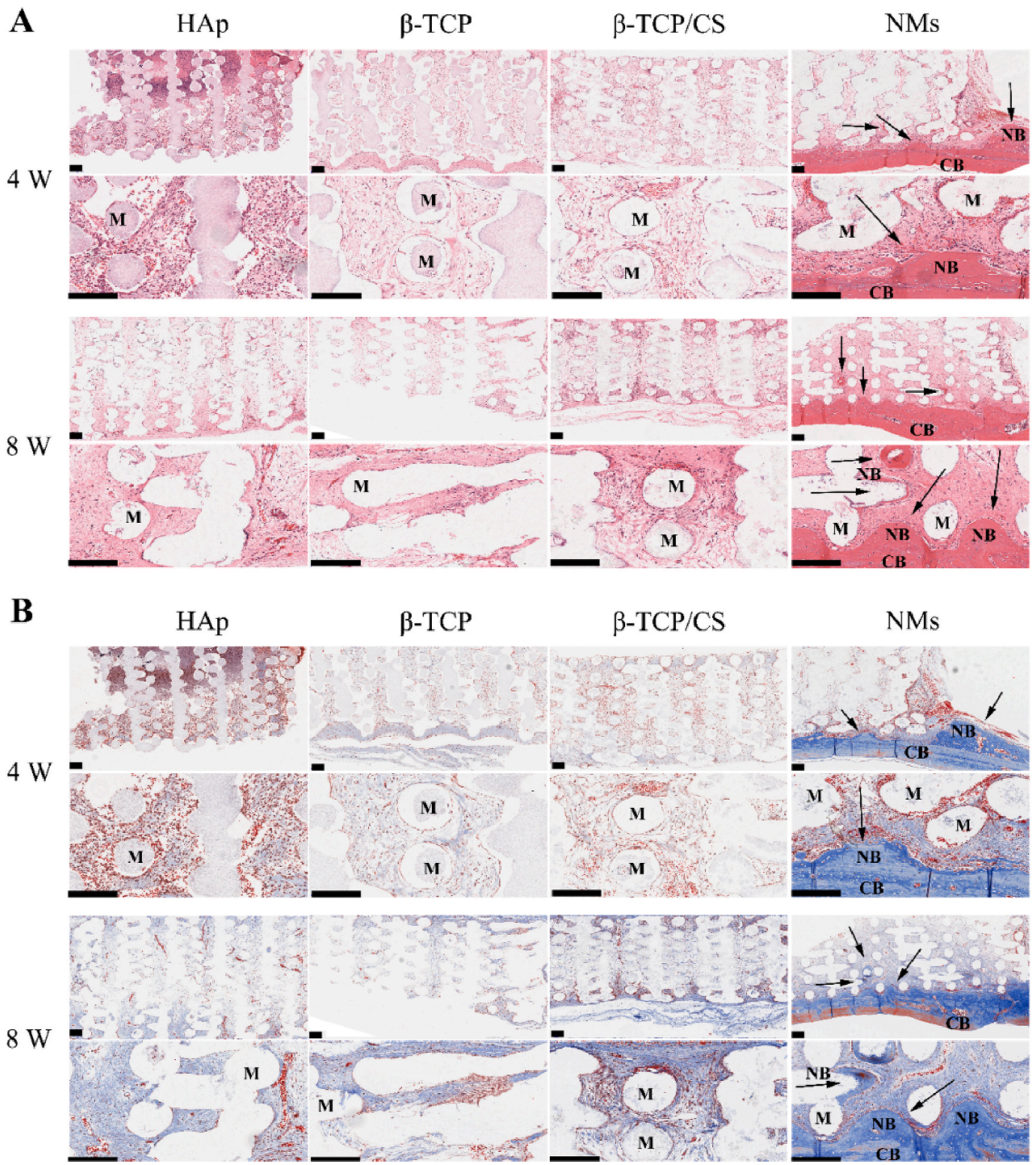

Fig. 6. (A) H&E staining of the HAp scaffold (Hs), β-TCP scaffold (Ts), β-TCP/$CaSiO_3$ scaffold (Os) and scaffold with a micro/nano-HAp surface layer (NMs). Scale bar 200 μm. (B) Masson staining of the HAp scaffold (Hs), β-TCP scaffold (Ts), β-TCP/$CaSiO_3$ scaffold (Os) and scaffold with a micro/nano-HAp surface layer (NMs). Scale bar 200 μm (M: materials, CB: cortical bone, NB: new bone matrix, black arrows indicate osteogenesis).

the scaffolds were harvested at 8 weeks, especially in the NMs group. As a result, few capillaries existed by H&E staining after implantation for 8 weeks. Masson staining showed that a small amount of Col-I was secreted in the ectopic subcutaneous environment. The Masson staining results of capillary formation were consistent with the H&E staining results. To summarize, considerable capillaries formed on the NMs scaffolds after 4 weeks but regressed after 8 weeks. In addition, immunohistochemical staining for CD31 of SD rat subcutaneous implants in the backs was performed (ESI Fig. 4). From the H&E staining and Masson staining results, capillary vessels formed at 4 weeks (but regressed at 8 weeks), while CD31 staining showed no significant differences between groups, and CD31 positivity faded at 8 weeks. Ectopic

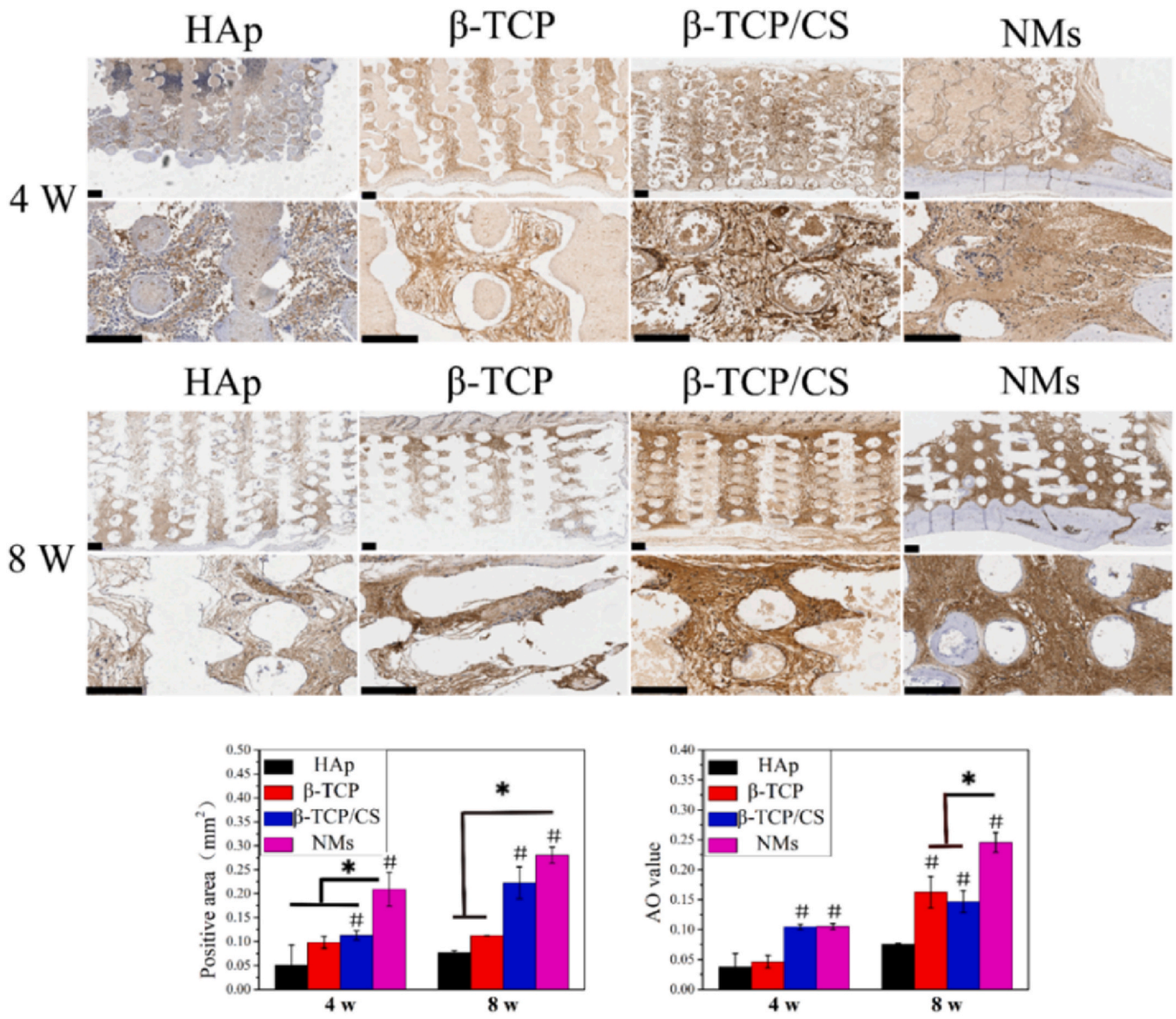

Fig. 7. OCN staining of the HAp scaffold (Hs), β-TCP scaffold (Ts), β-TCP/$CaSiO_3$ scaffold (Os) and scaffold with a micro/nano-HAp surface layer (NMs). Scale bar 200 μm.

implantation might not form substantial bone or vessels since integration with the artery could not be achieved.

4. Discussion

The scaffolds with interconnected pores were fabricated by 3D printing technology, and the interconnected porous architecture was conducive to tissue ingrowth and cellular migration. Uniform micro/nano-rod HAp was constructed on the surface of scaffolds via hydrothermal treatment. No organic agent or supersaturation mineral solution was utilized in the hydrothermal treatment [20]; as a result, the obtained HAp layer contained negligible amounts of the impurity phase via XRD measurement, and the surface elemental composition was relative pure, with a Ca/P ratio of approximately 1.60. The "Posner cluster" is a sub-nanometre cluster with a chemical composition of $Ca_9(PO_4)_6$ and exhibits an amorphous calcium phosphate (ACP) precursor phase [11]; therefore, the Ca/P ratio might change constantly as the ACP precursor phase changes to a more stable phase (such as HAp). In addition, the basic unit of the apatite crystals tends to stick to the c plane rather than make up the whole crystal at one time, causing the Ca/P ratio to range from 1.5 (Posner cluster) to 1.667 (flawless HAp). Moreover, compared to sintered HAp, the HAp crystals synthesized by hydrothermal treatment have relatively poor crystallinity [10]. Therefore, the obtained HAp structured surface regulated by hydrothermal treatment might be similar to that of natural bone, whose inorganic crystal composition is mainly apatite with poor crystallinity [29,39]. To summarize, the fabricated biomimetic hierarchical structure scaffolds exhibited characteristics of a micro/nano-HAp surface layer and interconnected porous architecture.

Based on a previous study, the formation process of the micro/nano-structure on the surface involved dissolution-precipitation: Rather than mineral ions deposited on the substrate directly, the original scaffolds initially dissolved and released mineral ions into the surroundings. The released mineral ions accumulated in the Stern layer of the substrate and re-crystalized at the active site on the surface; hence, the specific surface area of NMs increased as well as the surface micro- and meso-pore volume increased (from the BET results). Since $CaSiO_3$ was proved to be capable of inducing bone-like apatite formation in supersaturated

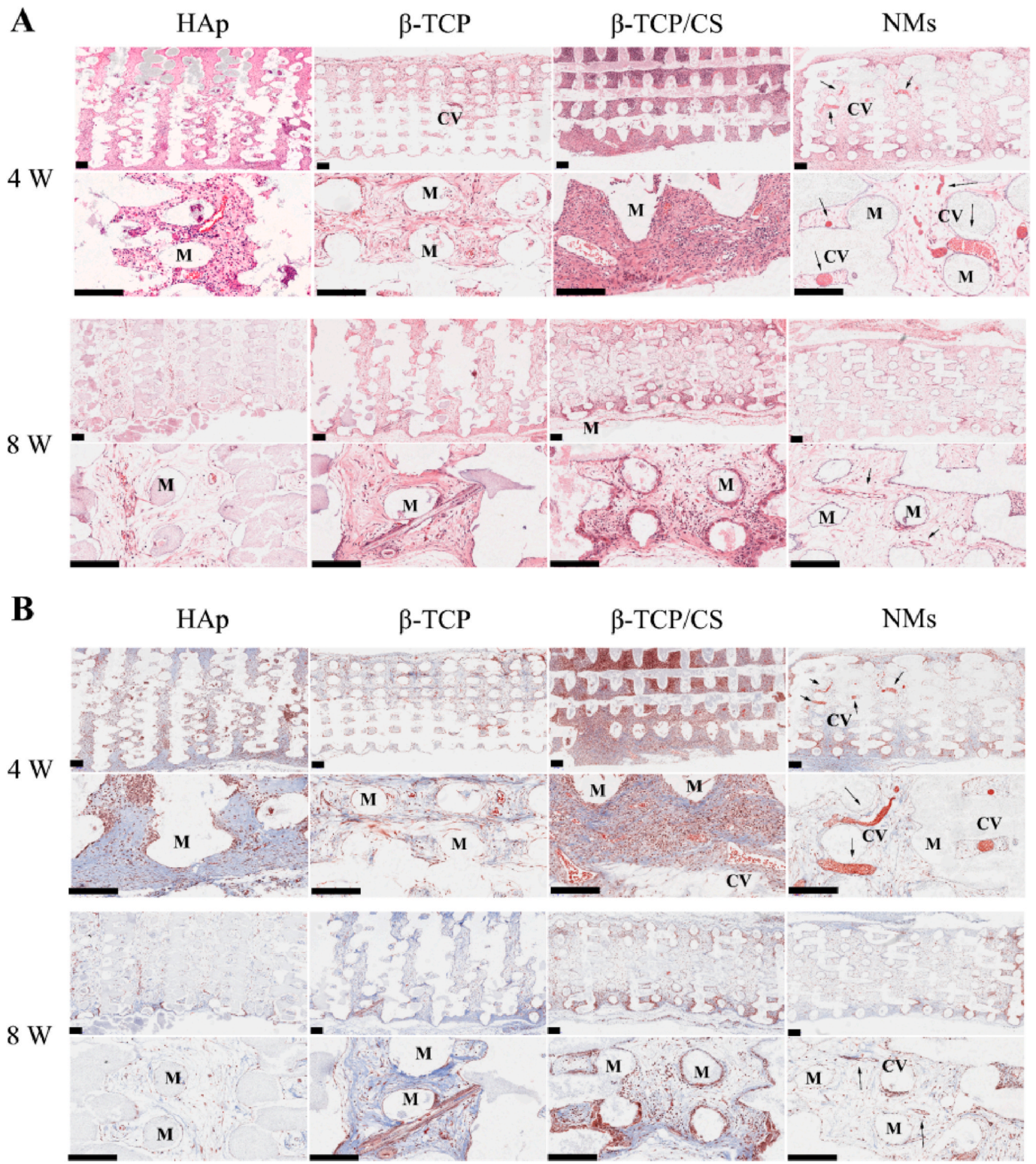

Fig. 8. (A) H&E staining of HAp scaffold (Hs), β-TCP scaffold (Ts), β-TCP/$CaSiO_3$ scaffold (Os) and scaffold with a micro/nano-HAp surface layer (NMs). Scale bar 200 μm.. (B) Masson staining of HAp scaffold (Hs), β-TCP scaffold (Ts), β-TCP/$CaSiO_3$ scaffold (Os) and scaffold with a micro/nano-HAp surface layer (NMs). Scale bar 200 μm. (M: materials, CV: capillary vessel, black arrows indicate CVs).

mineralization solution and the rate was more rapid than that of bioglass or A-W glass ceramics [22], the silica-rich surface favoured the accumulation of mineralization and could be regarded as the active site for heterogeneous nucleation; some nanoscale "pellets" on the surface of crystals were observed (via TEM), and these nano-clusters might be the building units of crystal growth and consist of "Posner clusters" [12], which might indicate that crystal growth occurred through the accumulation of crystal units rather than direct phase transformation [40].

As HAp was bioactive and biomimetic relative to natural bones, the biological effects on the cellular behaviour were tested. Integrin is a transmembrane receptor that is crucial for cell adhesion. Compared to original pre-treatment scaffolds (Os) and HAp scaffolds (Hs), 3D

scaffolds with a HAp surface micro/nano-hybrid structure layer (NMs) upregulated the gene expression of the integrin subunit, which indicated that the obtained micro/nano-HAp surface might favour cell adhesion. In addition, mBMSCs tended to grow together and were mainly distributed on the obtained micro/nano-HAp surface (ESI Fig. 1 and F-actin staining in Fig. 4). Even though no significant differences were observed in mBMSCs proliferation among the groups, the proliferation of HUVECs inhibited by Os. Since the burst release of $CaSiO_3$ leading the acute pH rise in microenvironment which might hinder the proliferation of the endothelial cells [41]. As a consequence, although studies proved the element release of Ca, P and Si might be contribute to proliferation of stem cells [42], the mineral ion release showed no advantage in proliferation of HUVECs in this study.

For the osteogenic differentiation of mBMSCs, the osteogenic markers ranged from early stage to anaphase. The zinc-finger-structure osteogenic transcription factor OSX is one of the promoter genes during osteogenesis [43]. Osteopontin (OPN) is an intermediate marker that has been proven to be associated with mature osteoblasts [44]. OCN is common gene marker that emerges at the late stage of osteogenic differentiation, which regulates bone matrix deposition and is usually associated with bone mineralization [45]. Collagen-I is an important component of bones and is crucial to biomineralization [46]. The PCR results indicated that ion release (silica) favoured the gene expression of osteogenic factors, especially in early stage, while the surface structure showed significant effect after culturing for 14 d; these results suggest that the obtained micro/nano-HAp surface layer might contribute more to osteogenic gene expression with prolonged culture time. In addition, the osteogenic differentiation of target protein secretion was upregulated in NMs, and the immunofluorescence results of OCN were consistent with gene expression, which indicated that the obtained micro/nano-HAp surface layer could promote the osteogenic differentiation of mBMSCs *in vitro*.

Regarding the effects on the gene expression of HUVECs, the target gene markers including CD31, KDR, TGF-β and VEGF were tested. Vascular endothelial growth factor (VEGF) not only dominates the proliferation and differentiation of endothelial cells but can also guide the germination of blood vessels and form lumen [47]. Transforming growth factor (TGF-β) can regulate the release of VEGF. The kinase regional receptor (KDR), also known as endothelial growth factor receptor (VEGFR-2), promotes the formation of lymphatic and vascular cells [48]. Platelet-endothelial cell adhesion molecule (CD31), also known as PECAM-1, regulates endothelial cell adhesion and is involved in endothelial cell migration, angiogenesis, and integrin activation [49]. The relative gene expression levels of CD31 and KDR in Ts were higher than those in Os, while the relative gene expression levels of VEGF and TGF-β in Os were higher. However, CD31, KDR, TGF-β and VEGF expression was more upregulated in the NMs group than in the Os and Ts groups. Although it was reported that Si could favour the angiogenesis of stem cells [48], the released mineral ions showed negligible effects on the gene expression of HUVECs. It is rational to speculate that the obtained micro/nano-HAp surface layer promotes the gene expression of HUVECs rather than the released mineral ions. In addition, the results of immunofluorescent in CD31 supported that speculation. To summarize, the obtained micro/nano-HAp surface layer constructed on the biomimetic hierarchical structure scaffolds promoted the target gene expression of mBMSCs and HUVECs *in vitro*.

In vivo ectopic subcutaneous implantation was performed on the backs of SD rats. Considerable capillaries contained evident haemocytes formed on the surface of NMs (4 weeks) but regressed since the capillaries could not be integrated with the artery (8 weeks); this result indicated that NMs promoted the formation of capillaries in an ectopic environment but that forming substantial vessels might be subject to the microenvironment *in vivo*. A more intriguing phenomenon was observed when scaffolds were implanted onto the periosteum in the skull of SD rats. In some clinical situations [35], bone repair materials are required to form new bone out of cortical bone to achieve bone augmentation. Significant bone augmentation in the NMs group was observed at the bone–implant interface after implantation for 4 weeks. New bone matrix was found surrounding the margin of the scaffolds in 4 weeks but did not emerge at the site distant from the bone–implant interface. When harvested after implanting for 8 weeks, a certain amount of new bone matrix could be found in the site distant from the bone–implant interface, which might be due to cell migration to the site. From the *in vivo* study, biomimetic hierarchical structure scaffolds with a micro/nano-HAp surface layer could form bonds to bone. In addition, when the biomimetic hierarchical structure scaffolds were set onto the periosteum in which stem cells and endothelial cells resided [50], the promotion of bone augmentation and bone formation might be associated with mediating cell fate. As shown in the *in vitro* study, the obtained micro/nano-HAp surface layer regulates cell fate, leading to osteogenesis and angiogenesis *in vivo*.

Referring to previous studies and others' reports, the reason why the biomimetic hierarchical structure scaffolds could promote bone regeneration *in vivo* might be speculated as follows: (1) Mediation of cell fate to angiogenesis and osteogenesis *in vitro*. It was reported that the micro/nano-HAp layer favoured the cellular differentiation of stem cells and promoted osteogenesis [6,12]. In addition to in this study, we found that the obtained micro/nano-HAp surface layer could not only favour the cell adhesion and differentiation of mBMSCs but also promote the angiogenesis of HUVECs. (2) The stable HAp surface with a biodegradable substrate. Although bio-degradability and releasing mineralization ions could favour osteogenesis, a stable surface was still needed to facilitate bone formation [51,52]. In this study, the substrates (β-TCP and $CaSiO_3$) were bio-degradable ceramics, while the HAp surface layer was a stable surface for bone formation and could promote osseointegration of the scaffolds since the inorganic component of bone is apatite. The biomimetic hierarchical structure scaffolds with a stable surface and biodegradable substrate might balance the match of tissue growth and degradability of implants. (3) HAp surface layer constructed on 3D-printed scaffolds with interconnected porous architecture. Dense bulk HAp was proved to lack osteogenesis activity *in vivo* [12]. The porous architecture was crucial for bone regeneration [13,53], so the 3D-printed scaffolds with interconnecting pores were ideal substrates for surface modification and might be conducive to osteogenesis and angiogenesis *in vivo*. Hence, the biomimetic hierarchical structure scaffolds could induce new bone formation out of cortical bone to achieve bone augmentation rather than just promoting osseointegration. In addition, it was reported that bone bonding involves micro-mechanical interdigitation of the bone tissue with the implant surface [54], and there is a highly conserved extracellular interfacial matrix called the "cement line", which has evolved to anchor new bone tissue; this "cement line" at the implant interfaces is involved in CaP nucleation and cluster crystal growth, with the crystal structure resembling that of the obtained micro/nano-HAp [54], so the next step of this investigation might focus on the effect of the morphology and size of the micro/nano-HAp layer on mediating cell fate.

5. Conclusions

In this study, a facile method of surface mineralization combined with 3D bioplotting technology was utilized to fabricate a biomimetic hierarchical structure scaffold. The biomimetic hierarchical structure scaffolds were fabricated with interconnected porous scaffolds as the architecture and micro/nano-HAp as the surface layer. The micro/nano-HAp surface layer favoured the adhesion and osteogenic differentiation of mBMSCs as well as the angiogenic gene expression of HUVECs. In addition, the results from *in vivo* study with ectopic subcutaneous implantation confirmed that the biomimetic hierarchical structure scaffolds promoted capillary formation and bone augmentation after being implanted for 4 weeks and induced new bone matrix formation in the site away from the bone–implant interface after being implanted for 8 weeks. This study might provide a practical strategy to design

biomimetic hierarchical structure scaffolds for bone regeneration and oral repair.

CRediT authorship contribution statement

Xiao Liu: Conceptualization, Methodology, Investigation, Writing – original draft, Data curation. **Yali Miao:** Methodology, Investigation, Writing – review & editing. **Haifeng Liang:** Investigation, Writing – review & editing. **Jingjing Diao:** Writing – review & editing. **Lijing Hao:** Investigation, Writing – review & editing. **Zhifeng Shi:** Writing – review & editing. **Naru Zhao:** Conceptualization, Resources, Writing – review & editing. **Yingjun Wang:** Conceptualization, Writing – review & editing, Supervision, Funding acquisition, Project administration.

Declaration of competing interest

There are no conflicts to declare.

Acknowledgements

This work was financially supported by the National key research and development plan (Grant No.2017YFC1105000, Grant No.2017YFA0205600), Outstanding Scholar Program of Guangzhou Regenerative Medicine and Health Guangdong Laboratory (2018GZR110102001), the Science and Technology Program of Guangdong Province (Grant No.2019B010941002), the Science and Technology Program of Guangzhou (Grant No.201804020060, Grant No.202007020002), Natural Science Foundation of Guangdong Province (Grant No.2021A1515011741, 2020A1515011354), the National Nature Science Foundation of China (Grants U1801252), National Natural Science Foundation of China (31700823), Guangzhou Science and Technology Planning Project (202102020005).

Appendix A. Supplementary data

Supplementary data to this article can be found online at https://doi.org/10.1016/j.bioactmat.2021.10.016.

Data availability

The data used in the present study are available from the corresponding author on reasonable request.

References

[1] Y. Chen, Z. Sun, Y. Li, Y. Hong, Osteogenic commitment of mesenchymal stem cells in apatite nanorod-aligned ceramics, ACS Appl. Mater. Interfaces 6 (2014) 21886–21893, https://doi.org/10.1021/am5064662.
[2] L.E. McNamara, R.J. McMurray, M.J. Biggs, F. Kantawong, R.O. Oreffo, M.J. Dalby, Nanotopographical control of stem cell differentiation, J. Tissue Eng. 2010 (2010) 120623, https://doi.org/10.4061/2010/120623.
[3] L. Lv, Y. Tang, P. Zhang, Y. Liu, X. Bai, Y. Zhou, Biomaterial cues regulate epigenetic state and cell functions-a systematic review, Tissue Eng. B Rev. 24 (2018) 112–132, https://doi.org/10.1089/ten.teb.2017.0287.
[4] W. Chen, L.G. Villa-Diaz, Y. Sun, S. Weng, J.K. Kim, R.H. Lam, L. Han, R. Fan, P. H. Krebsbach, J. Fu, Nanotopography influences adhesion, spreading, and self-renewal of human embryonic stem cells, ACS Nano 6 (2012) 4094–4103, https://doi.org/10.1021/nn3004923.
[5] E.K. Yim, E.M. Darling, K. Kulangara, F. Guilak, K.W. Leong, Nanotopography-induced changes in focal adhesions, cytoskeletal organization, and mechanical properties of human mesenchymal stem cells, Biomaterials 31 (2010) 1299–1306, https://doi.org/10.1016/j.biomaterials.2009.10.037.
[6] L. Xia, K. Lin, X. Jiang, B. Fang, Y. Xu, J. Liu, D. Zeng, M. Zhang, X. Zhang, J. Chang, Z. Zhang, Effect of nano-structured bioceramic surface on osteogenic differentiation of adipose derived stem cells, Biomaterials 35 (2014) 8514–8527, https://doi.org/10.1016/j.biomaterials.2014.06.028.
[7] S.W. Ha, J. Park, M.M. Habib, G.R. Beck Jr., Nano-hydroxyapatite stimulation of gene expression requires fgf receptor, phosphate transporter, and Erk1/2 signaling, ACS Appl. Mater. Interfaces 9 (2017) 39185–39196, https://doi.org/10.1021/acsami.7b12029.
[8] X. Zhang, H. Li, C. Lin, C. Ning, K. Lin, Synergetic topography and chemistry cues guiding osteogenic differentiation in bone marrow stromal cells through ERK1/2 and p38 MAPK signaling pathway, Biomater. Sci. 6 (2018) 418–430, https://doi.org/10.1039/c7bm01044c.
[9] Z. Jahed, S. Molladavoodi, B.B. Seo, M. Gorbet, T.Y. Tsui, M.R. Mofrad, Cell responses to metallic nanostructure arrays with complex geometries, Biomaterials 35 (2014) 9363–9371, https://doi.org/10.1016/j.biomaterials.2014.07.022.
[10] T. Lecuit, P.F. Lenne, Cell surface mechanics and the control of cell shape, tissue patterns and morphogenesis, Nat. Rev. Mol. Cell Biol. 8 (2007) 633–644, https://doi.org/10.1038/nrm2222.
[11] X. Yao, R. Peng, J. Ding, Cell-material interactions revealed via material techniques of surface patterning, Adv. Mater. 25 (2013) 5257–5286, https://doi.org/10.1002/adma.201301762.
[12] K. Lin, L. Xia, J. Gan, Z. Zhang, H. Chen, X. Jiang, J. Chang, Tailoring the nanostructured surfaces of hydroxyapatite bioceramics to promote protein adsorption, osteoblast growth, and osteogenic differentiation, ACS Appl. Mater. Interfaces 5 (2013) 8008–8017, https://doi.org/10.1021/am402089w.
[13] R.Z. LeGeros, Calcium phosphate-based osteoinductive materials, Chem. Rev. 108 (2008) 4742–4753, https://doi.org/10.1021/cr800427g.
[14] A.J. Xie, Y.H. Shen, C.Y. Zhang, Z.W. Yuan, X.M. Zhu, Y.M. Yang, Crystal growth of calcium carbonate with various morphologies in different amino acid systems, J. Cryst. Growth 285 (2005) 436–443, https://doi.org/10.1016/j.jcrysgro.2005.08.039.
[15] W. Wang, Y. Oaki, C. Ohtsuki, T. Nakano, H. Imai, Formation of c-axis-oriented columnar structures through controlled epitaxial growth of hydroxyapatite, J. Asian Ceram. Soc. 1 (2018) 143–148, https://doi.org/10.1016/j.jascer.2013.03.009.
[16] G. Wang, Z. Lu, X. Zhao, A. Kondyurin, H. Zreiqat, Ordered HAp nanoarchitecture formed on HAp-TCP bioceramics by "nanocarving" and mineralization deposition and its potential use for guiding cell behaviors, J. Mater. Chem. B 1 (2013) 2455–2462, https://doi.org/10.1039/c3tb20164c.
[17] L. Xia, N. Zhang, X. Wang, Y. Zhou, L. Mao, J. Liu, X. Jiang, Z. Zhang, J. Chang, K. Lin, B. Fang, The synergetic effect of nano-structures and silicon-substitution on the properties of hydroxyapatite scaffolds for bone regeneration, J. Mater. Chem. B 4 (2016) 3313–3323, https://doi.org/10.1039/c6tb00187d.
[18] X. Guo, X. Liu, H. Gao, X. Shi, N. Zhao, Y. Wang, Hydrothermal growth of whitlockite coating on β-tricalcium phosphate surfaces for enhancing bone repair potential, J. Mater. Sci. Technol. 34 (6) (2018) 1054–1059, https://doi.org/10.1016/j.jmst.2017.07.009.
[19] L. Bai, Z. Du, J. Du, W. Yao, J. Zhang, Z. Weng, S. Liu, Y. Zhao, Y. Liu, X. Zhang, X. Huang, X. Yao, R. Crawford, R. Hang, D. Huang, B. Tang, Y. Xiao, A multifaceted coating on titanium dictates osteoimmunomodulation and osteo/angio-genesis towards ameliorative osseointegration, Biomaterials 162 (2018) 154–169, https://doi.org/10.1016/j.biomaterials.2018.02.010.
[20] X. Liu, N. Zhao, X. Guo, H. Duan, J. Diao, Y. Dong, Y. Wang, Construction of a micro/nano structured surface on a β-TCP/CaSiO3 bioceramic promotes osteogenic differentiation of mBMSCs, CrystEngComm 21 (2019) 513–523, https://doi.org/10.1039/c8ce01711e.
[21] M. Bohner, J. Lemaitre, Can bioactivity be tested in vitro with SBF solution? Biomaterials 30 (2009) 2175–2179, https://doi.org/10.1016/j.biomaterials.2009.01.008.
[22] L.H. Long, L.D. Chen, S.Q. Bai, J. Chang, K.L. Lin, Preparation of dense β-CaSiO3 ceramic with high mechanical strength and HAp formation ability in simulated body fluid, J. Eur. Ceram. Soc. 26 (2006) 1701–1706, https://doi.org/10.1016/j.jeurceramsoc.2005.03.247.
[23] P. Siriphannon, Y. Kameshima, A. Yasumori, K. Okada, S. Hayashi, Formation of hydroxyapatite on CaSiO3 powders in simulated body fluid, J. Eur. Ceram. Soc. 22 (2002) 511–520, https://doi.org/10.1016/s0955-2219(01)00301-6.
[24] P. Habibovic, H. Yuan, C.M. van der Valk, G. Meijer, C.A. van Blitterswijk, K. de Groot, 3D microenvironment as essential element for osteoinduction by biomaterials, Biomaterials 26 (2005) 3565–3575, https://doi.org/10.1016/j.biomaterials.2004.09.056.
[25] A.V. Do, B. Khorsand, S.M. Geary, A.K. Salem, 3D printing of scaffolds for tissue regeneration applications, Adv. Healthc. Mater. 4 (2015) 1742–1762, https://doi.org/10.1002/adhm.201500168.
[26] J.L. Jameson, D.L. Longo, Precision medicine–personalized, problematic, and promising, N. Engl. J. Med. 372 (2015) 2229–2234, https://doi.org/10.1056/NEJMsb1503104.
[27] J. Diao, J. OuYang, T. Deng, X. Liu, Y. Feng, N. Zhao, C. Mao, Y. Wang, 3D-plotted beta-tricalcium phosphate scaffolds with smaller pore sizes improve in vivo bone regeneration and biomechanical properties in a critical-sized calvarial defect rat model, Adv. Healthc. Mater. 7 (2018), e1800441, https://doi.org/10.1002/adhm.201800441.
[28] Y. Dong, H. Duan, N. Zhao, X. Liu, Y. Ma, X. Shi, Three-dimensional printing of β-tricalcium phosphate/calcium silicate composite scaffolds for bone tissue engineering, Bio-Des. Manuf. 1 (2018) 146–156, https://doi.org/10.1007/s42242-018-0010-5.
[29] S. Weiner, W. Traub, H.D. Wagner, Lamellar bone: structure-function relations, J. Struct. Biol. 126 (1999) 241–255, https://doi.org/10.1006/jsbi.1999.4107.
[30] S.K. Ramasamy, A.P. Kusumbe, L. Wang, R.H. Adams, Endothelial Notch activity promotes angiogenesis and osteogenesis in bone, Nature 507 (2014) 376–380, https://doi.org/10.1038/nature13146.
[31] C. Zhu, S. Pongkitwitoon, J. Qiu, S. Thomopoulos, Y. Xia, Design and fabrication of a hierarchically structured scaffold for tendon-to-bone repair, Adv. Mater. 30 (2018), e1707306, https://doi.org/10.1002/adma.201707306.
[32] J. Kim, W.G. Bae, H.W. Choung, K.T. Lim, H. Seonwoo, H.E. Jeong, K.Y. Suh, N. L. Jeon, P.H. Choung, J.H. Chung, Multiscale patterned transplantable stem cell

patches for bone tissue regeneration, Biomaterials 35 (2014) 9058–9067, https://doi.org/10.1016/j.biomaterials.2014.07.036.
[33] S.W. Kuo, H.I. Lin, J.H. Ho, Y.R. Shih, H.F. Chen, T.J. Yen, O.K. Lee, Regulation of the fate of human mesenchymal stem cells by mechanical and stereo-topographical cues provided by silicon nanowires, Biomaterials 33 (2012) 5013–5022, https://doi.org/10.1016/j.biomaterials.2012.03.080.
[34] A.I. Caplan, Mesenchymal stem cells: time to change the name, Stem Cells Transl. Med. 6 (2017) 1445–1451, https://doi.org/10.1002/sctm.17-0051.
[35] F. Zhao, W. Xie, W. Zhang, X. Fu, W. Gao, B. Lei, X. Chen, 3D printing nanoscale bioactive glass scaffolds enhance osteoblast migration and extramembranous osteogenesis through stimulating immunomodulation, Adv. Healthc. Mater. 7 (2018), e1800361, https://doi.org/10.1002/adhm.201800361.
[36] A. Singh, A. Daing, V. Anand, J. Dixit, Two dimensional alveolar ridge augmentation using particulate hydroxyapatite and collagen membrane: a case report, J. Oral Biol. Craniofac. Res. 4 (2014) 151–154, https://doi.org/10.1016/j.jobcr.2014.01.002.
[37] F. Pieri, E. Lucarelli, G. Corinaldesi, N.N. Aldini, M. Fini, A. Parrilli, B. Dozza, D. Donati, C. Marchetti, Dose-dependent effect of adipose-derived adult stem cells on vertical bone regeneration in rabbit calvarium, Biomaterials 31 (2010) 3527–3535, https://doi.org/10.1016/j.biomaterials.2010.01.066.
[38] F. Zhao, W. Xie, W. Zhang, X. Fu, W. Gao, B. Lei, X. Chen, 3D printing nanoscale bioactive glass scaffolds enhance osteoblast migration and extramembranous osteogenesis through stimulating immunomodulation, Adv Healthc Mater 7 (2018), e1800361, https://doi.org/10.1002/adhm.201800361.
[39] S. Weiner, H.D. Wagner, The material bone: structure-mechanical function relations, Annu. Rev. Mater. Sci. 28 (1998) 271–298, https://doi.org/10.1146/annurev.matsci.28.1.271.
[40] W.J. Habraken, J. Tao, L.J. Brylka, H. Friedrich, L. Bertinetti, A.S. Schenk, A. Verch, V. Dmitrovic, P.H. Bomans, P.M. Frederik, J. Laven, P. van der Schoot, B. Aichmayer, G. de With, J.J. DeYoreo, N.A. Sommerdijk, Ion-association complexes unite classical and non-classical theories for the biomimetic nucleation of calcium phosphate, Nat. Commun. 4 (2013) 1507, https://doi.org/10.1038/ncomms2490.
[41] D. Zhang, M. Hupa, L. Hupa, In situ pH within particle beds of bioactive glasses, Acta Biomater. 4 (2008) 1498–1505, https://doi.org/10.1016/j.actbio.2008.04.007.
[42] Y. Zhou, C. Wu, J. Chang, Bioceramics to regulate stem cells and their microenvironment for tissue regeneration, Mater, Today Off. 24 (2019) 41–56, https://doi.org/10.1016/j.mattod.2018.07.016.
[43] T. Koga, Y. Matsui, M. Asagiri, T. Kodama, B. de Crombrugghe, K. Nakashima, H. Takayanagi, NFAT and Osterix cooperatively regulate bone formation, Nat. Med. 11 (2005) 880–885, https://doi.org/10.1038/nm1270.
[44] G.R. Beck Jr., B. Zerler, E. Moran, Phosphate is a specific signal for induction of osteopontin gene expression, Proc. Natl. Acad. Sci. U.S.A. 97 (2000) 8352–8357, https://doi.org/10.1073/pnas.140021997.
[45] N.K. Lee, H. Sowa, E. Hinoi, M. Ferron, J.D. Ahn, C. Confavreux, R. Dacquin, P. J. Mee, M.D. McKee, D.Y. Jung, Z. Zhang, J.K. Kim, F. Mauvais-Jarvis, P. Ducy, G. Karsenty, Endocrine regulation of energy metabolism by the skeleton, Cell 130 (2007) 456–469, https://doi.org/10.1016/j.cell.2007.05.047.
[46] P. Habibovic, D.C. Bassett, C.J. Doillon, C. Gerard, M.D. McKee, J.E. Barralet, Collagen biomineralization in vivo by sustained release of inorganic phosphate ions, Adv. Mater. 22 (2010) 1858–1862, https://doi.org/10.1002/adma.200902778.
[47] G.D. Yancopoulos, S. Davis, N.W. Gale, J.S. Rudge, S.J. Wiegand, J. Holash, Vascular-specific growth factors and blood vessel formation, Nature 407 (2000) 242–248, https://doi.org/10.1038/35025215.
[48] H. Li, K. Xue, N. Kong, K. Liu, J. Chang, Silicate bioceramics enhanced vascularization and osteogenesis through stimulating interactions between endothelia cells and bone marrow stromal cells, Biomaterials 35 (2014) 3803–3818, https://doi.org/10.1016/j.biomaterials.2014.01.039.
[49] C. Betsholtz, Vascular biology: transcriptional control of endothelial energy, Nature 529 (2016) 160–161, https://doi.org/10.1038/nature16866.
[50] X. Shi, T. Fujie, A. Saito, S. Takeoka, Y. Hou, Y. Shu, M. Chen, H. Wu, A. Khademhosseini, Periosteum-mimetic structures made from freestanding microgrooved nanosheets, Adv. Mater. 26 (2014) 3290–3296, https://doi.org/10.1002/adma.201305804.
[51] P. Habibovic, M.C. Kruyt, M.V. Juhl, S. Clyens, R. Martinetti, L. Dolcini, N. Theilgaard, C.A. van Blitterswijk, Comparative in vivo study of six hydroxyapatite-based bone graft substitutes, J. Orthop. Res. 26 (2008) 1363–1370, https://doi.org/10.1002/jor.20648.
[52] P. Habibovic, K. de Groot, Osteoinductive biomaterials–properties and relevance in bone repair, J. Tissue Eng. Regen. Med. 1 (2007) 25–32, https://doi.org/10.1002/term.5.
[53] W. Habraken, P. Habibovic, M. Epple, M. Bohner, Calcium phosphates in biomedical applications: materials for the future? Mater. Today 19 (2016) 69–87, https://doi.org/10.1016/j.mattod.2015.10.008.
[54] J.E. Davies, Bone bonding at natural and biomaterial surfaces, Biomaterials 28 (2007) 5058–5067, https://doi.org/10.1016/j.biomaterials.2007.07.049.